OUR NEWEST RESULTS ON THE FIELD OF STRUCTURAL OPTIMIZATION

Károly Jármai[1], József Farkas[2], György Kovács[3], Zoltán Virág[3]
[1] Prof.Dr. [2] Prof. Emeritus. [3] Assoc.Prof. University of Miskolc, Hungary

1. INTRODUCTION

The optimum design process has the following three main phases:
(a) preparation: selection of candidate structural versions defining the main characteristics to be changed, formulation of design constraints and cost function,
(b) solution of the constrained function minimization problem by using efficient mathematical methods,
(c) evaluation of results by designers, comparison of optimized versions, formulation of design rules, incorporation in expert systems.
These phases show that the structural optimization has the following three main parts: cost function, design and fabrication constraints, and mathematical method.
The following examples show how to elaborate these phases.

2. OPTIMIZATION OF WELDED SQUARE CELLULAR PLATES WITH TWO DIFFERENT KINDS OF STIFFENERS

Cellular plates consist of two face plates and a grid of stiffeners welded between them. In the present study, these rolled stiffeners are used. The comparison of the cellular plates with this stiffener shows that using optimization significant savings in mass and cost can be achieved.

2.1. Bending moments and deflections

The cells produce a large torsional stiffness; thus, the cellular plates can be calculated as isotropic ones (Figure 1). Cellular plates have some advantages over stiffened ones as follows. (a) their torsional stiffness contributes to the overall buckling strength significantly, therefore, their dimensions (height and thickness) can be smaller, (b) their symmetry eliminates the large residual welding distortions, which can occur in stiffened plates due to shrinkage of eccentric welds. Therefore cellular plates can be cheaper than stiffened ones. Lee et al. [1] have solved the differential equation for rectangular orthotropic plates supported at four corners by using a polynomial function.
Formulae have given for bending moments and deflections as a function of bending and torsional stiffnesses. In the case of a square cellular plate, the bending stiffnesses are equal to the torsional stiffness ($B_x = B_y = H$) and the maximum bending moment is

$$M_{max} = 0.15pL^2 \tag{1}$$

and the maximum deflection is expressed by

$$w_{max} = 0.025p_0L^4/B_x \tag{2}$$

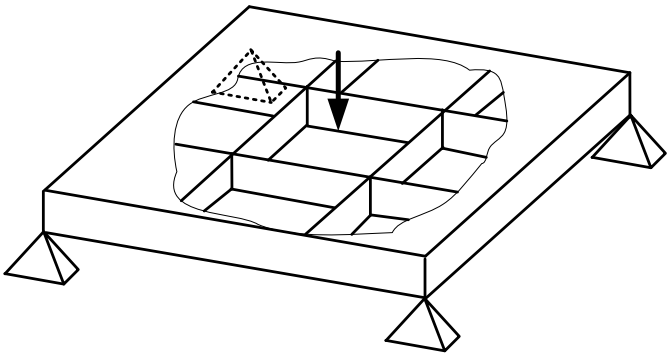

Figure 1. A cellular plate supported at four corners

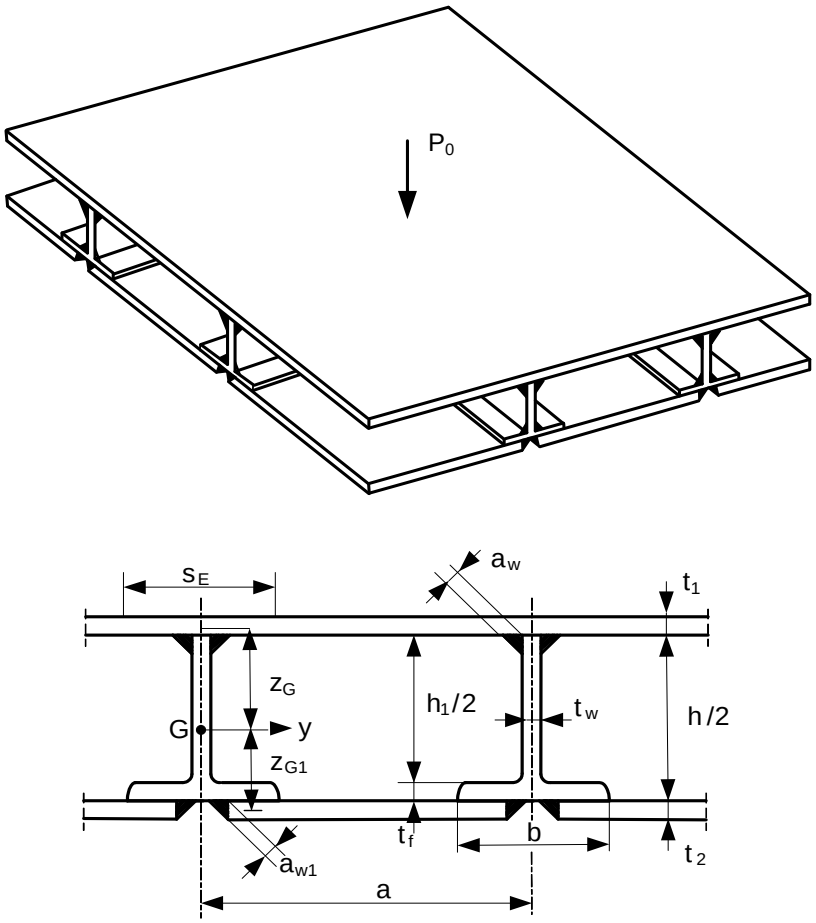

Figure 2. Cellular plate and dimensions of halved rolled I-section stiffener

where L is the plate edge length, p_0 is the factored intensity of the uniformly distributed normal load and p is the load intensity including the self mass of the plate.

Results for square isotropic plates according to Timoshenko & Woinowsky-Krieger [2]

for $\nu = 0.3$ $$M_{max} = 0.1404pL^2 \quad (3)$$

and $$w_{max} = 0.0249p_0L^4/B_x \quad (4)$$

It can be seen that the constants are nearly the same.

2.2. Cellular plate with halved rolled I-section stiffeners (Figure 2)

2.2.1. Design constraints

Stress constraint including normal stress due to local bending of an upper base plate part with built-in edges according to Timoshenko & Woinowsky-Krieger [2]

$$\sigma_P = 0.0513\frac{p_0 a^2}{t_1^2/6} = 0.3078\frac{p_0 a^2}{t_1^2} \tag{5}$$

$$\sigma_2 = \frac{0.15 p L^2 z_G}{I_y} + \sigma_P \le \frac{f_y}{1.1} \tag{6}$$

Constraint on stress in the lower face plate

$$\sigma_1 = \frac{0.15 p L^2 z_{G1}}{I_y} \le \frac{f_y}{1.1} \tag{7}$$

Deflection constraint

$$w_{max} = \frac{0.025 p_0 L^4}{B_x} \le w_{allow} = \frac{L}{300} \tag{8}$$

Shear stress constraint at the corners

$$\tau = \frac{pL^2}{4h_1 t_w} \le \frac{f_y}{1.1\sqrt{3}} \tag{9}$$

2.2.2. Fabrication constraints

Thickness limitation: t_{min} = 4 mm. Limitation of the distance between stiffener flanges to allow the welding of the stiffener web to the upper base plate:

$$a - b \ge 300 \text{ mm}. \tag{10}$$

2.2.3. Structural variables

- number of stiffeners in one direction (square symmetry) *n*,
- thicknesses of the upper and bottom base plates t_1 and t_2,
- height of the rolled I-section stiffener *h*.

2.2.4. Numerical data

Plate edge length: L = 18 m, factored load intensity p_0 = 150 kg/m^2 = 0.0015 N/mm^2, yield stress of steel f_y = 355 MPa, elastic modulus E = 2.1x10^5 MPa, Poisson ratio v = 0.3, steel density ρ = 7.85x10^{-6} kg/mm^3, ρ_0 = 7.85x10^{-5} N/mm^3.

2.2.5. Cost function

The cost function is formulated according to the fabrication sequence [3].

(a) Welding of the upper base plate (18x18 m) from 36 pieces of size 6 m x 1.5 m using single or double bevel welds with complete joint penetration (GMAW-C gas metal arc welding with CO_2)

(b) Welding of n+2 continuous stiffeners to the upper base plate by double fillet welds (GMAW-C)

(c) Welding of n+2 intermittent stiffeners to the upper base plate and to the continuous stiffeners (webs with fillet welds, flanges with butt welds GMAW-C)

(d) Welding of the bottom plate parts to the flanges of stiffeners by fillet welds (GMAW-C)

Cost of material

$$K_M = k_M \rho V_4, \quad k_M = 1 \text{ \$/kg}, \tag{11}$$

Cost of painting

$$K_P = k_P \Theta_P S_P, \Theta_P = 3, \quad k_P = 14.4\text{x}10^{-6} \text{ \$/mm}^2 \tag{12}$$

surface to be painted

$$S_P = 3L^2 + 2L(h_1 + b)(n+2) \tag{13}$$

Total cost

$$K = K_M + K_{w1} + K_{w2} + K_{w3} + K_{w4} + K_P \tag{14}$$

2.2.6. Optimization and results

A systematic search for the optima is performed using a MathCAD algorithm. The results are given in Table 1.

Table 1. Results of a systematic search. Halved rolled I-stiffeners. The optima are marked by bold letters. Allowed normal stress (σ_2) 322 MPa, allowed deflection $w_{\max}$ = 60 mm. Dimensions in mm

h	n	t_1	t_2	σ_2 MPa	$w_{\max}$ mm	Vx10^{-9} mm^3	Kx10^{-5} \$
683.5	4	11	4	286	38	6.766	1.273
	5	9	4	315	40	6.435	1.258
	6	8	4	317	41	6.429	1.286
607.6	3	13	4	311	49	6.791	1.253
	4	**11**	**4**	316	50	6.400	**1.224**
	5	10	4	302	50	6.332	1.240
	6	9	4	302	51	6.265	1.258
	7	**8**	**4**	313	52	**6.197**	1.277
533.1	3	14	5	312	55	7.200	1.292
	4	12	5	314	57	6.761	1.255
	5	11	5	298	57	6.646	1.263
	6	10	5	296	58	6.530	1.272

2.3.5. Comparison of the optimized cellular plate

It has been shown in previous studies that, in the case of square symmetry, the torsional stiffness of cellular plates equals to their bending stiffness. Thus, they can be calculated as isotropic ones and the bending moments and deflection for a square plate supported at four corners can be obtained by using the formulae for isotropic plates.

In the optimization process the four variables are as follows: height and number of halved rolled I-section stiffeners. A systematic search considers the constraints on stresses and deflection, as well as the cost function to be minimized.
According to the results summarized in Table 1 it can be concluded that the cellular plate the optima for cost and mass minima are different. It can be up to 10% saving in mass (volume).

3. OPTIMAL DESIGN OF A COMPOSITE SANDWICH STRUCTURE BY PARTICLE SWARM OPTIMIZATION METHOD

3.1. A new cellular sandwich plate model

Our new structural model combines the sandwich and cellular plates, since it has *FRP* (fiber reinforced plastic) deck plates and more aluminium square hollow section stiffeners riveted into the deck plates. So it is a new combination of materials, stiffeners and fabrication technology, which results a high ratio of bending stiffness to density.
The sandwich plate model under consideration is depicted in Figure 3. The *CFRP* plates are constructed from laminated layers. Plates are riveted to the upper and lower flanges of the aluminium square hollow section (*SHS*) profiles.

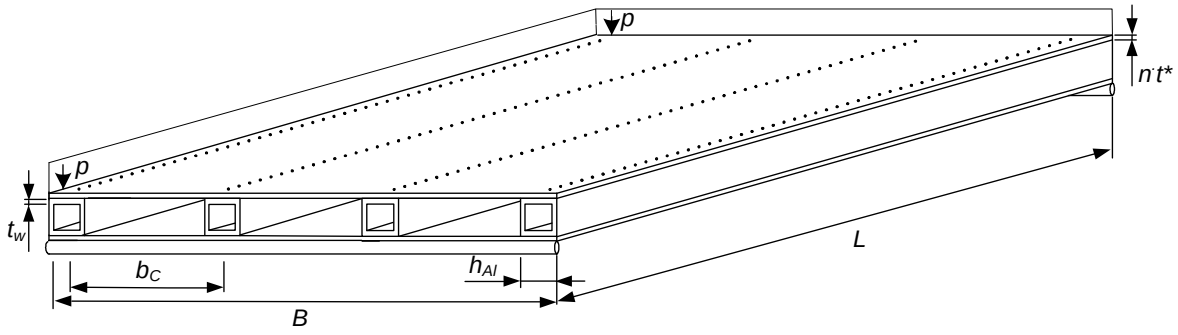

Figure 3. Cellular sandwich plate structure.

The structure is simply supported, and a uniformly distributed loading of $3{,}5 \cdot 10^{-3}$ N/mm^2. (p = 7 N/mm line pressure) acts on the total surface of the structure. The dimensions of the structure are: L = 2250 mm, B = 2000 mm.
The material parameters of a pre-impregnated *CFRP* layer are given as follows: the thickness of a layer t^* = 0,2 mm, the longitudinal Young's modulus $E_x = E_c$ =120 GPa and the transverse modulus E_y = 9 GPa. The specific mass of the *CFRP* plate ρ_c = 180 g/m^2, and Poisson's ratios ν_{xy} = 0,25 and ν_{yx} = 0,019.

3.2. Objective functions and constraints

3.2.1. Cost function

The structure is optimized with respect to minimum cost K, which can be formulated as the sum of the material and manufacturing costs, i.e.

$f(x) = K = K_{CFRP} + K_{Al} + K_{heat\ treatment} + K_{manufacturing}$

$$K\ (€) = 2\cdot(n\cdot 31{,}047) + k_{Al}\,[n_s\,(\rho_{Al}\,4\,h_{Al}\,t_w\,L)] + 2\,n\,k_{ht} + k_f\,[n\cdot 14_{\min} + n_s\cdot 26_{\min} + 110_{\min}] \quad (15)$$

where n represents the number of *CFRP* layers, n_s the number of stiffeners, ρ_{Al} the density of the *Al* profile, h the height and t_w thickness of the SHS *Al* profiles.
In our case the material cost of composite plates is cost reached 31,047 Euro/layer. The cost of the *Al* profile is 4,94 Euro/kg. The specific fabrication cost k_f =0,6 €/min. The cost of heat treatment is k_{ht} =1 Euro/layer.
The total fabrication cost (as the function of time [min]) is the sum of the cost required for the manufacturing of the *CFRP* plates, the cutting cost of the *Al* profiles and the total assembly costs.

3.2.2. Mass function

The total cost of the structure is the sum of the *CFRP* and *Al* components:

$$m = 2\,\rho_c\,[B\,L(\,n\,t^*)] + n_s\,\rho_{Al}\,[L\,(4\,h_{Al}\,t_w - 4\,t_w^2)] \quad (16)$$

3.2.3. Constraints

3.2.3.1. Deflection of the total structure

$$w_{\max} = \frac{5p\,L^4}{384(E_c I_c + E_{AL} n_s I_{AL})} + \frac{5\Delta M\,L^2}{48(E_c I_c + E_{AL} n_s I_{AL})} \le \frac{L}{200} \quad (17)$$

where: I_c, I_{Al}: moment of inertia of the *CFRP* plate and *Al* profile,
E_c, E_{Al}: reduced modulus of elasticity of the *CFRP* lamina and Young's modulus of *Al* profile.
There is the effect of the relative movement between the components, and is expressed as a function of the differences in predicted stresses in the middle of *Al* profile and *CFRP* plate. Due to difference in stress $(\Delta\sigma)$ there is a corresponding difference in the equivalent applied moment (ΔM).

3.2.3.2. Composite plate buckling [4]

$$\left(\frac{b_c}{nt^*}\right) \le \sqrt{\frac{\pi^2}{6\sigma_{\max}\left(1-\nu_{xy}\nu_{yx}\right)}\left[\sqrt{E_x E_y} + E_x\nu_{xy} + 2G_{xy}\left(1-\nu_{xy}\nu_{yx}\right)\right]} \quad (18)$$

where b_c: plate width between stiffeners, σ_{max}: maximal stress in the *CFRP* lamina E_x, E_y, G_{xy}: laminate moduli, ν_{xy}, ν_{yx}: Poisson's ratios.

3.2.3.3. Web buckling in the Al profiles [5,6]

$$\frac{h_{Al}}{t_w} \le 42\sqrt{\frac{235E_{Al}}{240E_{Steel}}} \quad (19)$$

where: E_{Al}, E_{Steel}: Young's modulus of elasticity of *Al* and *Steel*.

3.2.3.4. Stress in the composite plates

The moment acting on the total structure is distributed on the components of the structure. X_cM is the part of total moment which is acting on composite plate, $X_{Al}M$ is the part of total moment which is acting on stiffeners.

$$\frac{X_c M}{I_c} \cdot \frac{h_{Al} + nt}{2} \leq \sigma_{Call} \tag{20}$$

where: $X_c = \frac{E_c I_c}{E_{Al} n_s I_{Al} + E_c I_c}$; $M = \frac{pL^2}{8}$; $\sigma_{Call} = \frac{\sigma_T}{\gamma_c}$: allowable stress, X_cM: moment acting on composite plate, σ_T: tensile strength of composite lamina, γ_c: safety factor (=2).

3.2.3.5. Stress in the Al stiffeners

$$\frac{X_{Al} M}{n_s I_{Al}} \cdot \frac{h_{Al}}{2} \leq \sigma_{Alall} \tag{21}$$

where: $X_{Al} = \frac{E_{Al} n_s I_{Al}}{E_{Al} n_s I_{Al} + E_c I_c}$; $\sigma_{Alall} = \frac{f_y}{\gamma_{Al}}$: allowable stress, $X_{Al}M$: moment acting on *Al* tube, f_y: yield stress of *Al*, γ_{Al}: safety factor (=2).

3.2.3.6. Eigenfrequency of the total structure

$$f_1 = \frac{\pi}{2L^2} \sqrt{\frac{10^3 (E_{Al} I_{Al} + E_k I_k)}{m}} \geq f_0 \tag{22}$$

m: weight/unit length of the structure [kg/m], f_0: limitation for eigenfrequency (50 Hz).

3.2.3.7. Size constraints for design variables

$$\begin{gathered} 10 \leq h_{Al} \leq 100 \\ 2 \leq t_w \leq 6 \\ 16 \leq n \leq 32 \\ 7 \leq n_s \leq 20 \end{gathered} \tag{23}$$

These represent physical limitations on the design variables [mm], taking economical and manufacturing aspects into consideration.

3.3. Particle Swarm Optimization method

During the Particle Swarm Optimization [7] the normalized weighting method were used to show the weight of the cost- and mass objective functions. The normalized objectives method solves the problem of the pure weighting method e.g. at the pure weighting method, the weighting coefficients do not reflect proportionally the relative importance of the objective, because of the great difference on the nominal

value of the objective functions. At the normalized weighting method we reflect closely the importance of objectives.

$$f(\boldsymbol{x}) = \sum_{i=1}^{r} w_i f_i(\boldsymbol{x}) / f_i^0 \qquad \text{where } w_i \geq 0 \text{ and } \sum_{i=1}^{r} w_i = 1 \quad (24)$$

The condition $f_i^0 \neq 0$ is assumed.

3.4. Numerical results of multiobjective optimization

We used sensitivity analysis to determine how sensitive the structure is to changes in the value of the parameters of the model and to changes in the structure of the model. Different values of many parameters were set to see how a change in the parameters causes a change in the optimal structural construction.
At first design variables were analysed in aspect of sensitivity in case of the 20, 22, 24, 26 layered plate structures [8, 9].
It can be realised that design variables have no significant effect on value of objective functions. After that we analysed the other components of the objective functions. We have found that the optimal solution is very sensitive to changing of specific fabrication cost (k_f).
We completed the multiobjective optimization for case of different values (1; 2; 2.5; 3; 4 times higher value) of specific fabrication cost to present the effect of sensitivity.
Table 2 includes the result of optimization completed for 26 layered deck plate structure.

Table 2. Result of Particle Swarm Optimization

	Weights of objective functions	h_{Al} **[mm]**	t_w **[mm]**	n_s **[mm]**
k_f **[Euro/min]**	100-0%	60	2,5	8
$2 \cdot k_f$ **[Euro/min]**	0-100%	50	3	9
	50-50%	50	3	9
	80-20%	50	3	9
	90-10%	55	3	8
	95-5%	60	3	8
	100-0%	70	3	7
$2{,}5 \cdot k_f$ **[Euro/min]**	100-0%	80	4	6
$3 \cdot k_f$ **[Euro/min]**	100-0%	85	4	6
$4 \cdot k_f$ **[Euro/min]**	100-0%	90	4	6
	Cost-mass objective functions			

Table 2 includes the optimal structure alternatives for 26 layered deck plate model. Table 2 summarises the optimal stiffener number and stiffener geometries in case of different value of specific fabrication cost and different weight of objective functions. The first number of weight (2. column of Table 2) represents the effect of cost function in percentage, the second number represents the weight of mass objective function in the multiobjective optimization.

4. EXPERIENCE OF WEARING OF THE NEW WELDED BUCKET AND CUTTING TOOTH OF BUCKET LADDER EXCAVATOR

This chapter briefly outlines the operative wearing results of an optimized cutting tooth. The description of the rock cutting process is very complex. Thus the investigation of the effect of lateral forces was complicated through cutting tests. A finite element analysis of cutting tooth was presented in which the linear increase of the lateral force is taken into consideration. The simulation results have shown that the maximum stresses decrease if the lateral force increases. Operative results show the correctness of the simulation. This design process and results are summarized in this paper [10, 11].

4.1. Development of the aggrading channel and the digging ladder

Design of the new construction of bucket excavator the exchangeability, the placement of the teeth and the form of the aggrading channel represent constraints, and it is important to take into account the manufacturability and better breakage. Based on these polygonal flat plates the cutting edge, cutting edge supporters and digging ladder back side designed to be simpler and more accurate for manufacturing and refurbishment. On this way a more precise digging ladder can be manufactured (Figure 4).

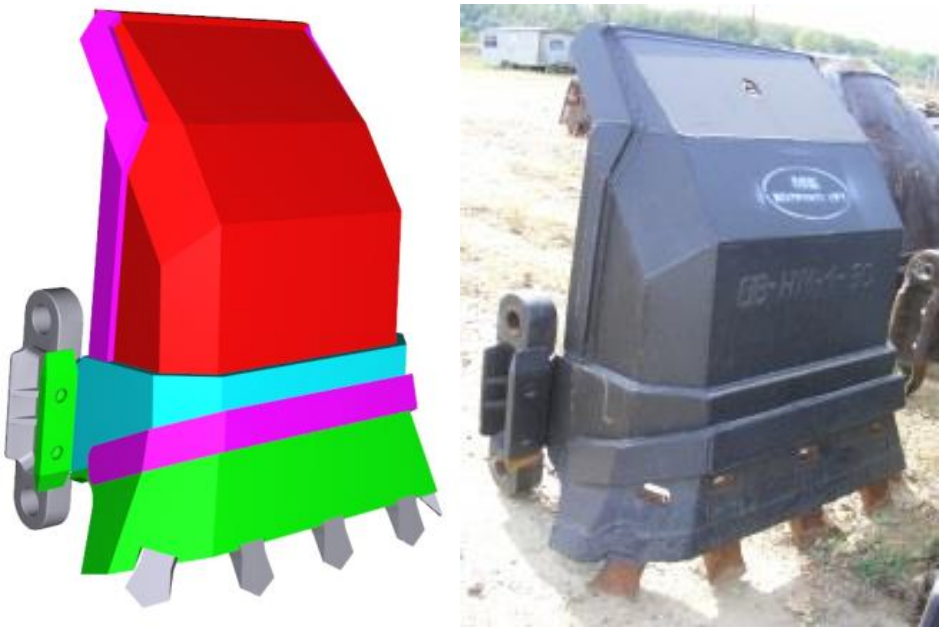

Figure 4. 3D model of the new digging ladder

In order to achieve the goals of the development, a lot of monitoring, data acquisition, planning, design, etc. had to be done on a coordinated way to reach a new uniform digging ladder with changeable teeth. We had to take into account the applied technology from the point of view of the breakage as well as the aspect of geometry in terms of energy, and the changeability and the refurbishment. Theoretical and technological studies have shown that a digging ladder has a

complex motion performed during breakage. Digging ladder has a parabolic move in yawing during every moment of the orientation there is an angle between the breakage to the digging ladder [12].
The developed finite element model gave the stress distribution in the digging ladder as it is visible on Figure 5.

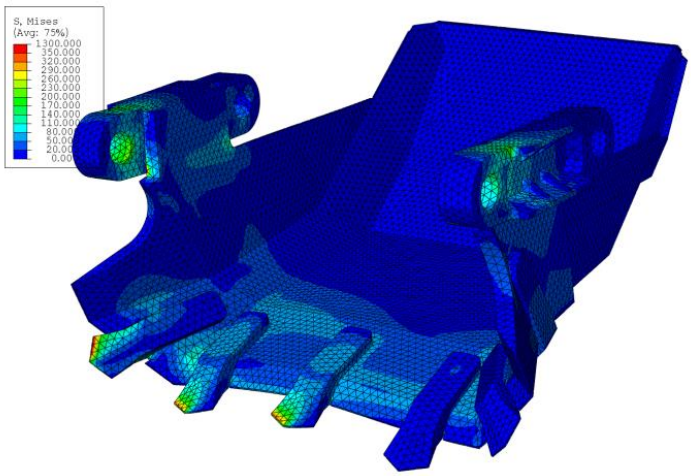

Figure 5. Reduced stress distribution in the new digging ladder

The higher strength digging ladder has less detrimental deformation, and expected to be less technical problems.
The lower specific cutting force requires less drive performance, as well as the smaller side forces, the power consumption of the translation will be less. The welded edge protectors of the cutting teeth increase its life.

5. CONCLUSIONS

There were three different applications shown in this paper. These applications demonstrate the applicability and the efficiency of the optimization.
In the first application the cellular plates with two face plates and a grid of stiffeners welded between them are optimized. In the present study, these rolled stiffeners are used. The comparison of the cellular plates with this stiffener shows that using optimization significant savings in mass and cost can be achieved.
The second application is the new structural model combines the sandwich and cellular plates, since it has *FRP* (fiber reinforced plastic) deck plates and more aluminium square hollow section stiffeners riveted into the deck plates. So it is a new combination of materials, stiffeners and fabrication technology, which results a high ratio of bending stiffness to density. We have shown the efficiency of this structure is load carrying applications.
In the third application the optimized cutting tooth is shown. A finite element analysis of cutting tooth was presented in which the linear increase of the lateral force is taken into consideration. The simulation results have shown that the maximum stresses decrease if the lateral force increases. Operative results show the correctness of the simulation.

Acknowledgement

The research was supported by the TÁMOP 4.2.4.A/2-11-1-2012-0001 priority project entitled 'National Excellence Program - Development and operation of domestic personnel support system for students and researchers, implemented within the framework of a convergence program, supported by the European Union, co-financed by the European Social Fund. The research was supported also by the Hungarian Scientific Research Fund OTKA T 109860 project and was partially carried out in the framework of the Center of Excellence of Innovative Engineering Design and Technologies at the University of Miskolc.

References

[1] LEE SL, KARASHUDI P, ZAKERIA M, CHAN KS (1971). **Uniformly loaded orthotropic rectangular plate supported at the corners**. *Civil Engineering Transactions,* Institution of Engineering Australia, 13(2): 101-106.

[2] TIMOSHENKO S, WOINOWSKY-KRIEGER S. (1959) **Theory of plates and shells**. 2nd ed. New York-Toronto-London: McGraw-Hill.

[3] FARKAS J, JÁRMAI K. **Optimum design of steel structures** (2013), Springer Verlag, Heidelberg, 288 p. ISBN 978-3-642-36867-7, http://dx.doi.org/10.1007/978-3-642-36868-4

[4] BARBERO E. J. (1999) **Introduction to composite materials design,** USA: Taylor & Francis

[5] FARKAS, J.; JÁRMAI, K. (1997) **Analysis and optimum design of metal structure**, Balkema: Rotterdam-Brookfield.

[6] FARKAS, J.; JÁRMAI, K. (1998) **Minimum material cost design of five-layer sandwich beams**. Structural Optimization 15 No.3-4, pp.: 215-220

[7] KENNEDY, J.; EBERHART, R. (1995) **Particle swarm optimization**, *Proc. of the 1995 IEEE International Conference on Neural Networks,* Perth, Australia, IEEE Service Center, Piscataway, NJ, **4,** pp.:1942-1948

[8] NOOR, A. K.; BURTON, W.S.; BERT, C. W. (1996) **Computational models for sandwich panels and shells**, Appl. Mech. Rev. 49 No. 3, pp.: 155-199

[9] VINSON, J. R. (2001) **Sandwich structures**, Appl. Mech. Rev. 54 No. 3, pp.: 201-214

[10] VIRÁG, Z. (2006) **Optimum design of stiffened plates**, Pollack Periodica, Vol. 1, No. 1, HU ISSN 1748-1994, pp. 77-92

[11] VIRÁG, Z. (2004) **Optimum design of stiffened plates for different loads *and* shapes *of* ribs**, Journal of Computational and Applied Mechanics, Volume 5, Number 1, HU ISSN 1586-2070, pp. 165-179

[12] VIRÁG, Z., SZIRBIK S. (2011): **The application of new uniform digging ladder with changeable teeth** (in Hungarian), *GÉP*, VOL. LXII. NO. 11. PP. 48-51. ISSN 0016-8572.